The use of sublimable chlorotricarbonyl bis(phenylimino)acenaphthene rhenium(I) complexes as photosensitizers in bulk-heterojunction photovoltaic devices

Chris S. K. Mak [a], Hei Ling Wong [a], Qing Yun Leung [a], Wing Yan Tam [a], Wai Kin Chan [a,*], Aleksandra B. Djurišić [b]

[a] Department of Chemistry, The University of Hong Kong, Pokfulam Road, Hong Kong

[b] Department of Physics, The University of Hong Kong, Pokfulam Road, Hong Kong

Abstract

A series of sublimable substituted chlorotricarbonyl bis(phenylimino) acenaphthene rhenium(I) complexes was synthesized and used in the fabrication of photovoltaic devices. The hole and electron carrier mobilities of these complexes are in the order of 10^{-3} to 10^{-4} $cm^2V^{-1}s^{-1}$. Heterojunction devices with CuPc/complex/C_{60} (CuPc = copper phthalocyanine) as the active layer and bulk heterojunction devices with complex:C_{60} as the active layer were fabricated. The rhenium complexes function as photosensitizer in the devices, and exhibit optical absorption in the region between 500-550 nm within which other components in the device do not absorb. Other devices with hole transport materials, exciton blocking materials, and different active layer thickness were also fabricated. Variation of substitution groups in the ligand did not show significant difference in device performance. The best power conversion efficiency of the devices was measured to be 1.29 % under illumination of AM1.5 simulated solar light.

Keywords: Rhenium(I) carbonyl complexes, photovoltaic devices, sensitizers

1. Introduction

Research in organic solar cells has attracted considerable interests in the past decade because of their potential applications as alternative light harvesting devices other than the conventional silicon-based solar cells.[1, 2] However, the performance and lifetime of most organic solar cells there are not satisfactory. In general, organic materials exhibit low carrier mobilities, low absorbance in near-IR region, short exciton diffusion length, and poor long-term stability. In order to improve the performance of organic photovoltaic devices, design of new photosensitizing/charge transport materials and fabrication of devices with improved architecture are essential.

Other than organic molecules, transition metal complexes have also been employed as photosensitizers for harvesting light energy, especially for dye-sensitized solar cells in which ruthenium complexes adsorb on the surface of an inorganic semiconducting materials.[3, 4] The applications of metal complexes and metal containing polymers for photovoltaic cells are also known.[5-11] Our group previously reported the use of different rhenium containing polymers for organic photovoltaic cell applications.[12, 13] However, there are only few examples of using rhenium complexes in DSSC[14] or organic solar cells. We developed a rhenium diimine complex that can function as photosensitizers in photovoltaic cells.[15, 16] In this paper, we report the synthesis of a series of chlorotricarbonyl rhenium complexes with different substituted bis(phenylimino)acenaphthene (DIAN) ligands.[17] The neutral complexes can be sublimed in vacuum, allowing them to be purified and processed into multilayer organic photovoltaic cells. The effects of varying the structure of the

ligands and device structure to photovoltaic device performances were investigated.

<Scheme 1>

<Figure 1>

2. Results and Discussion

2.1. Synthesis and Properties of the Complexes

The substituted DIAN ligands **3a-e** were synthesized by the reaction between acenaphthenequinone **1** and the corresponding substituted aniline **2a-e** (Scheme 1).[18] Rhenium complexes **4a-e** were synthesized by refluxing the ligand with rhenium(I) pentacarbonyl chloride in toluene in good yield. All the Re(I) complexes exhibit good thermal stability. The decomposition temperatures of the complexes determined by thermal gravimetric analysis are at least 250-300 °C (Table 1). Reasonable decomposition temperature is the prerequisite for thermal evaporation of these materials under vacuum. All the complexes were characterized by ^{1}H, ^{13}C NMR, and FTIR spectroscopies and mass spectrometry. In their FTIR spectra, three very strong absorption bands are observed in the region between 1888 to 2028 cm^{-1}, which are assigned to the CO stretching of the rhenium carbonyl moieties with *facial* configuration. Both electron donating and withdrawing groups were introduced to the DIAN ligands. The UV-vis absorption spectra of some complexes are shown in Figure 1, and Table 1 summarizes the absorption maxima of different complexes in solid thin film and in different solvents. In general, these complexes exhibit two major absorption bands, of which the higher energy one at ca. 370 nm is assigned to the ligand-centered (LC, π-π*) transition of the DIAN ligand, while the lower energy one at ca. 500 nm is assigned to the metal-to-ligand charge transfer (MLCT,

5dπ(Re)–π*(DIAN)) transition. Introduction of an electron donating methoxy group to the ligand results in a significant red shift in LC transition and blue shift in the MLCT absorption peak compared to that of the unsubstituted Re(I) complex. In contrast, the presence of electron withdrawing trifluoromethyl groups results in slight red shift in the MLCT absorption. On the other hand, from Table 1, it can also be seen that the absorption peak maxima of these complexes exhibit solvatochromism. The observation suggests that the lower energy electronic transition has charge transfer character. Profound effect on the photophysical and electrochemical properties of the complexes with different substituents on the DIAN ligands was not observed. This may be due to the fact that the two phenyl rings are almost orthogonal to that of the acenaphthene ligand, resulting in little overlap between the molecular orbitals which significantly reduces the substitution effect of the ligands. Interestingly, the MLCT absorption peak of the series of the complexes show hypsochromic shift with an increase in the solvent polarity. The absorption maxima in CH_3CN solutions are in general shifted 50 nm towards higher energy than those of toluene solutions. The result reveals that the complexes exhibit negative solvatochromic effect and more polar character of the ground state.

The effect of the geometry of the complexes can also be seen from the electronic energy levels. The HOMO and LUMO levels of the complexes were determined by cyclic voltammetry by comparing the first oxidation and reduction potentials of the complexes with those of ferrocene internal standard,[19] and the data are summarized in Table 1. In general, all complexes exhibit very similar HOMO levels, which indicates that the HOMOs mainly localize at the rhenium center. On the contrary, substitution of electron withdrawing/donating groups varies the LUMO levels (from -3.73 eV for **4a** to -3.92 eV for **4e**). The change of LUMO energies with

different substituents is due to the fact that the electron withdrawing/donating groups have a great influence to the energy of the π* orbital of the ligand than that of the dπ orbital of the Re(I) metal centre. It is reported that the electron-withdrawing substituents on the diimine stabilizes the ligand π* level.[20] The decrease in absorption and LUMO energies of the complexes with electron withdrawing groups in our study (Table 1) is consistent with that of the literature reported.

<Table 1>

The effect of different substituents to the HOMO and LUMO was further investigated by theoretical calculations. DFT calculation of complex **4c** shows that the HOMO is largely localized at the rhenium center with some contribution from the carbonyl and chloride ligands (Figure 2), while LUMO delocalizes between rhenium center and the DIAN ligand. This further suggests that the lowest excited state is not a pure MLCT state, which is mixed with ligand center character. It can also be seen that for both MOs, the contribution from the phenyl moieties is very small, and that the substituents have little effect to the electronic properties of the complexes.

<Figure 2>

2.2. Charge Carrier Mobility

Understanding the charge carrier mobilities of the materials in photovoltaic cells is important to the design of high performance devices by optimizing the charge transport and minimizing the recombination losses. Free carriers may be extracted by the hole and electron transport layers more efficiently, which can minimize the charge recombination process. It has been demonstrated by us that some rhenium diimine complexes for light emitting devices exhibit bipolar charge transport character.[21] The hole and electron carrier mobilities of the complexes were determined by time-of-

flight experiment, and the results are summarized in Table 2. The complexes exhibit comparable hole and electron carrier mobilities of the order of 10^{-4} $cm^2V^{-1}s^{-1}$. It was shown that these complexes are able to act as charge transport species by the metal center oxidation (hole hopping) or by the ligand center reduction (electron hopping) processes.[22] It can be observed that the carrier mobilities of complex **4c** are higher than those of other complexes. However, the difference in the carrier mobilities between **4c** and other complexes cannot be correlated to the structure or HOMO/LUMO energy levels of the complexes. One possible explanation is that the mobilities are affected by the solid-state morphology of the materials. Further experimental works to support this argument will be needed. From these results, it is envisaged that after exciton generation, electrons will be captured by fullerene molecules, while holes may be transported via the complexes before reaching the hole transport layer.

<Table 2>

<Table 3>

2.3. Fabrication of Photovoltaic Cells

In preliminary studies, we first fabricated different heterojunction photovoltaic devices using complex **4c** as the photosensitizing material. Different hole transport materials including copper phthalocyanine (CuPc), *N*,*N*'-diphenyl-*N*,*N*'-di-*m*-tolyl-*p*-benzidine (TPD), and *N*,*N*'-diphenyl-*N*,*N*'-bis(1-naphthyl)-1,1'-biphenyl-4,4"-diamine (NPB) were used. The results are summarized in Table 3. Heterojunction devices with **4c** as the sensitizer show improved performance compared to those devices with CuPc/C_{60} active layer.[23] In addition, devices with CuPc hole transport layer show better performance than other hole transport materials, which may be due

to the higher HOMO levels of CuPc (-5.3 eV)[24] than those of TPD and NPB (-5.5 and -5.4 eV respectively).[24, 25] In addition, CuPc exhibits high absorbance in the visible region, which may contribute to photocurrent generation (see discussion below). The optimum thickness for CuPc layer is between 15 to 25 nm, and the highest efficiency measured was 0.11 %.

Bulk-heterojunction photovoltaic devices were fabricated by blending the donor- and acceptor in one single layer. There is much larger contact surface area between donor and acceptor. However, the amount of donor and acceptor has to be carefully controlled because it directly affects the formation of charge percolation pathways in the mixed layer. Bulk heterojunction photovoltaic cells with CuPc:C_{60} as the active layers have been reported, and the efficiencies are in the order of 1-2 %.[26-28] We fabricated different series of bulk heterojunction photovoltaic cells with the device configuration ITO/CuPc/**4c**:C_{60}/C_{60}/Al by varying the ratio between complex **4a** and C_{60} in the active layer. The thickness of the active layer in these devices was varied between 25 to 100 nm, and the data are summarized in Table 4. For all devices, when the active layer thickness is higher than 75 nm, the efficiencies of the devices decrease rapidly. For the device with **4c**:C_{60} ratio of 9:1, due to the small amount of electron transport material in the active layer, low fill factor and efficiency were measured. The optimum thickness of the active **4c**:C_{60} layer appears to be dependent on the **4c**:C_{60} ratio. For the devices with **4c**:C_{60} ratio of 1:9 and 3:7, highest efficiencies were obtained when the active layer thickness was 25 nm, while for the device with 1:1 **4c**:C_{60} ratio the optimum thickness for the active layer was 50 nm. Figure 3a shows the current-voltage characteristics of different device with different **4c**:C_{60} ratio. The energy levels of different materials in the device are shown in Figure 3b, which shows that after exciton dissociation, transport of electrons from the

complex to C_{60} and holes from complex to CuPc are favorable processes.

<Table 4>

<Figure 3>

For comparison purpose, complexes **4a**, **4b**, **4d**, and **4e** were fabricated into bulk-heterojunction photovoltaic cells ITO/CuPc/complex:C_{60} (1:1)/C_{60}/Al with active layer thickness of 50 nm. The device performance data are summarized in Table 5. It can be seen that substitution with electron donating (**4a**, **4b**) or withdrawing (**4d**, **4e**) groups did not result in significant effect to device efficiency, and the performance of these device measured are in the range 0.62 to 0.79 %.

<Table 5>

We then attempted to further optimize the device based on complex **4c** by varying the hole transport material (HTM) or by insertion of an exciton diffusion blocking layer (EBL) between C_{60} and metal electrode. For the hole transport layer, TPD, NPB, zinc phthalocyanine (ZnPc), and 4,4'-*N*,*N*'-dicarbazolyl-biphenyl (CBP) were used (Table 5, entries 6-9). For devices with TPD, NPB, and CBP as the HTM, the device efficiencies are lower than 0.1 % (entries 7-9), which is due to the low absorbance of these materials in the visible region. The device based on ZnPc showed the best performance among these four (FF = 0.51, η_p = 0.59 %). However, it is still slightly lower than that the device with CuPc as HTM. It has been demonstrated that insertion of EBL between electron acceptor and metal cathode in photovoltaic cells can improve device efficiency.[29] In our studies, devices with bathocuproine (BCP) and perylene-3,4,9,10-tetracarboxylic diimide (PTCDI) as the EBL were fabricated (entries 10-13). From Table 5, it can be seen that insertion of EBL did not result in any significant improvement in device efficiency. Poor performance was also observed in the device fabricated with PTCDI EBL. It is possible that for different

HBL, there exists an optimum thickness that has to be carefully controlled, and further investigation may be necessary.

In order to understand which functionality is responsible for the generation of photocurrent in the device, we measured the incident photon-to-electron conversion efficiency (IPCE) as the function of incident wavelength. IPCE is defined as the number of electron generated per incident photon, and is represented by

$$\text{IPCE } (\%) = \frac{1240 \times I_{SC}}{\lambda \times \Phi} \times 100\%,$$

where I_{sc} is the short circuit current density (in mA/cm^2), λ is the wavelength of incident light (in nm) and Φ is the light intensity (in mW/cm^2). Figure 4 shows the plot of IPCE vs. incident light wavelength for the bulk heterojunction device fabricated from **4c**. The absorption spectra of thin films of **4c** and CuPc are also shown for comparison. Maximum IPCE of 25 % is observed at 620 nm, and the curve is very similar to the absorption spectrum of CuPc. This strongly indicates that optical absorption by the CuPc layer also plays an important role in the photocurrent generation process. This may also explain the observations that devices fabricated from other HTMs (except ZnPc) showed poor performances. However, it should be emphasized that the rhenium complexes are also important to photocurrent generation. Complex **4c** strongly absorbs in the region between 450-500 nm, in which CuPc shows almost no absorption at all. The IPCEs measured are higher than 5 % in the entire visible region. This shows that the rhenium complexes and CuPc exhibit complementary absorption in the visible region, and more photons can be harvested as a result.

3. Conclusions

The use of sublimable rhenium diimine complexes based on

bis(phenylimino)acenaphthene ligands as the active materials in photovoltaic devices was demonstrated. Insertion of a rheniumcomplex:C_{60} blend as the active layer in the device resulted in significant improvement in device performance compared to those devices based on CuPc:C_{60} active layer. We attribute the improvement in performance to the fact that these complexes may play the role of photosensitizers and charge transport materials in the devices. The best power conversion efficiency was measured to be 1.29 %. The performance of the devices may be improved by the use of complexes with higher absorption coefficient and carrier mobilities, and further investigation in the photophysical properties of these complexes will be required.

4. Experimental

4.1. Materials

Acenaphthenequinone tech. (95 %) and zinc chloride (98 %) were purchased from ABCR. *p*-Anisidine was purchased from Merck KGaA. *p*-Toluidine (99 %) was purchased from Aldrich Chemical Co. 4-Aminobenzotrifluoride (99 %) was purchased from Acros Organics. 4-Fluoroaniline (99 %) and aniline (99+ %) were purchased from Lancaster Synthesis Ltd. Rhenium pentacarbonyl chloride (98 %) was purchased from Strem Chemicals. For thermal evaporation, copper phthalocyanine (sublimation grade, dye content 99 %) was purchased from Aldrich Chemical Co. Fullerene (> 99.5 %) was purchased from BuckyUSA. Aluminium wire (99.999 %) was purchased from Strem Chemicals. Unless otherwise specified, all the chemicals were used as received.

*4.2. Synthesis of ligands (3**a**-3**e**)*

*Synthesis of Bis(4-methoxyphenylimino)acenaphthene **3a**:*[1] A mixture of

acenaphthenequinone **1** (2.0 g, 11 mmol), anhydrous $ZnCl_2$ (3.0 g, 22 mmol), and *p*-anisidine **2a** (3.4 g, 28 mmol) was heated under reflux in glacial acetic acid (20 ml) for 1 h. The suspension was cooled to room temperature and the solid, bis(4-methoxyphenylimino)acenaphthene zinc chloride, was filtered off, washed with acetic acid (2 × 10 ml) and diethyl ether (4 × 20 ml), and then air-dried. It was then added to an aqueous potassium carbonate solution (25 g in 25 ml water) and the mixture was refluxed with vigorous stirring for 2 h. The mixture was cooled to room temperature and the solid was filtered off and washed with water (5 × 30 ml). The product was dried under vacuum and recrystallized with ethanol. The product was collected as red needle (3.4 g, 79 %). ^{1}H NMR (400 MHz, $CDCl_3$): δ 7.89 (d, J = 8.2 Hz, 2H), 7.40 (t, J = 7.8 Hz, 2H), 7.10 (m, 4H), 7.02 (m, 6H), 3.90 (s, 6H). ^{13}C NMR (75 MHz, $CDCl_3$): δ 161.6, 156.9, 144.9, 128.8, 127.6, 123.6, 119.8, 114.6, 55.5. MS (EI): *m/z*: 393 $[M]^+$.

Ligands **3b-3e** were synthesized by the same procedure as for **3a** using different substituted anilines **2d-e**.

Bis(4-methylphenylimino)acenaphthene ***3b***: (70 %). ^{1}H NMR (300 MHz, $CDCl_3$): δ 7.91 (d, J = 8.3 Hz, 2H), 7.40 (t, J = 7.3 Hz, 2H), 7.30 (m, 4H), 7.05 (d, J = 8.2 Hz, 4H), 6.95 (d, J = 7.2 Hz, 2H), 2.47 (s, 6H). ^{13}C NMR (75 MHz, $CDCl_3$): δ = 161.7, 149.6, 134.3, 131.6, 130.4, 129.1, 128.0, 124.3, 118.6, 21.5. MS (EI): *m/z*: 361 $[M]^+$.

Bis(phenylimino)acenaphthene ***3c***: (71 %) ^{1}H NMR (300 MHz, $CDCl_3$): δ 7.90 (d, J = 8.3 Hz, 2H), 7.48 (t, J = 7.8 Hz, 4H), 7.37 (t, J = 8.1 Hz, 2H), 7.14 (d, J = 7.8 Hz, 4H), 6.84 (d, J = 7.2 Hz, 2H). ^{13}C NMR (100 MHz, $CDCl_3$): δ 161.3, 151.8, 141.8, 131.2, 129.4, 129.0, 128.6, 127.7, 124.4, 124.0, 118.2; MS (EI): *m/z*: 333 $[M]^+$.

Bis(4-fluorophenylimino)acenaphthene ***3d***:[30] (65 %). ^{1}H NMR (400 MHz, $CDCl_3$): δ 7.93 (d, J = 8.2 Hz, 2H), 7.42 (t, J = 7.8 Hz, 2H), 7.19 (m, 4H), 7.10 (m, 4H), 6.94 (d, J = 7.3 Hz, 2H). ^{13}C NMR (75 MHz, $CDCl_3$): δ 162.2, 159.0, 148.0, 131.7, 129.7, 128.7, 128.1, 124.3, 120.2, 120.1, 116.9, 116.6; MS (EI): *m/z*: 369 $[M]^+$.

Bis((4-trifluoromethyl)phenylimino)acenaphthene ***3e***: (58 %). ^{1}H NMR (300 MHz, $CDCl_3$): δ 7.97 (d, J = 8.2 Hz, 2H), 7.76 (d, J = 8.3 Hz, 4H), 7.44 (t, J = 7.8 Hz, 2H), 7.23 (d, J = 8.2 Hz, 4H), 6.85 (d, J = 7.2 Hz, 2H). ^{13}C NMR (100 MHz, $CDCl_3$): δ 161.3, 154.4, 142.0, 131.3, 129.7, 127.9, 126.8, 124.2, 118.3; MS (EI): *m/z*: 469 $[M]^+$.

*4.3. Synthesis of Complexes (**4a-e**):*

Synthesis of chlorotricarbonyl bis(4-methoxyphenylimino)acenaphthene rhenium(I) ***4a***: Under a nitrogen atmosphere, a mixture of **3a** (0.8 g, 2 mmol) and rhenium pentacarbonyl chloride (0.8 g, 2 mmol) in toluene (15 ml) was heated under reflux for 24 h. After cooling, the solid was filtered off and washed with toluene, ether, and then dried under vacuum. The product was collected as brownish solid. (1.3 g, 87 %). T_d = 336 $^\circ$C; ^{1}H NMR (400 MHz, $CDCl_3$): δ = 8.05 (d, J = 8.2 Hz, 2H), 7.65 (m, 2H), 7.51 (t, J = 7.8 Hz, 2H), 7.32 (m, 2H), 7.17 (d, J = 7.3 Hz, 2H), 7.11 (dd, J = 1.5, 7.6 Hz, 2H), 3.96 (s, 6H); ^{13}C NMR (125 MHz, $CDCl_3$): δ = 196.0, 186.3, 159.6, 144.8, 142.2, 131.4, 130.9, 129.0, 128.5, 128.2, 126.4, 125.3, 124.6, 123.1, 121.7, 115.0, 55.6; FTIR (KBr pellet): ν = 2020, 1921, 1888 cm^{-1} (metal carbonyl CO stretching); UV/Vis ($CHCl_3$): λ_{max} (ε) = 493 nm (7200 dm^3/mol·cm); MS (FAB): *m/z* (%): 698 $[M]^+$, 663 $[M\text{-}Cl]^+$. Anal. Calc. for $C_{29}H_{20}N_2ClO_5Re$: C, 49.89; H, 2.89; N,

4.01;. Found: C, 49.66; H, 2.54; N, 4.17 %.

Chlorotricarbonyl bis(4-methylphenylimino)acenaphthene rhenium(I) ***4b****:* (83 %); ^{1}H NMR (300 MHz, $CDCl_3$): δ 8.07 (d, J = 8.3 Hz, 2H), 7.62 (d, J = 6.2 Hz, 2H), 7.52 (t, J = 7.8 Hz, 2H), 7.43 (d, J = 8.6 Hz, 4H), 7.11 (d, J = 7.3 Hz, 2H), 7.09 (d, J = 8 Hz, 2H), 2.53 (s, 6H). ^{13}C NMR (125 MHz, $CDCl_3$): δ 196.0, 186.2, 172.8, 146.6, 144.9, 138.6, 131.4, 131.0, 130.8, 130.3, 128.5, 126.3, 124.8, 121.3, 119.9, 21.4. FTIR (KBr pellet): ν 2026, 1920 cm^{-1} (metal carbonyl CO stretching). UV-vis ($CHCl_3$): λ_{max} (ε) = 499 nm (11000 dm^3 $mol^{-1}\cdot cm^{-1}$). MS (FAB-MS): *m/z*: 667 $[M]^+$, 632 $[M\text{-}Cl]^+$. Anal. Calc. for $C_{29}H_{20}N_2ClO_3Re$: C, 52.29; H, 3.03; N, 4.21. Found: C, 51.94; H, 2.88; N, 4.06 %.

Chlorotricarbonyl bis(phenylimino)acenaphthene rhenium(I) ***4c****:* (96 %). ^{1}H NMR (400 MHz, $CDCl_3$): δ 8.06 (d, J = 8.2 Hz, 2H), 7.73 (d, J = 8.3 Hz, 2H), 7.63 (t, J = 8.0 Hz, 4H), 7.51 (t, J = 7.3 Hz, 2H), 7.48 (d, J = 8.1 Hz, 2H), 7.38 (d, J = 8.1 Hz, 2H), 7.00 (d, J = 7.3 Hz, 2H). ^{13}C NMR 125 MHz, $CDCl_3$): δ 195.8, 186.0, 173.0, 148.9, 145.0, 131.4, 131.1, 130.4, 129.9, 129.0, 128.6, 128.2, 126.2, 124.8, 121.3, 120.0. FTIR (KBr pellet): ν 2019, 1921 cm^{-1} (metal carbonyl CO stretching). UV-vis ($CHCl_3$): λ_{max} (ε) = 503 nm (7500 dm^3 $mol^{-1}cm^{-1}$); MS (FAB-MS): *m/z*: 638 $[M]^+$, 603 $[M\text{-}Cl]^+$. Anal. Calc. for $C_{27}H_{16}N_2ClO_3Re$: C, 50.82; H, 2.53; N, 4.39. Found: C, 50.43; H, 2.21; N, 4.11 %.

Chlorotricarbonyl bis(4-fluorophenylimino)acenaphthene rhenium(I) tricarbonyl chloride ***4d***: (90 %). ^{1}H NMR (300 MHz, $CDCl_3$): δ 8.10 (d, J = 8.2 Hz, 2H), 7.57 (m, 2H), 7.54 (td, J = 1.1, 7.8 Hz, 2H), 7.30 (m, 6H), 7.07 (d, J = 7.3 Hz, 2H); ^{13}C NMR

(125 MHz, $CDCl_3$): δ 195.6, 185.7, 173.4, 163.2, 161.2, 145.1, 144.9, 131.5, 131.4, 129.6, 128.7, 126.0, 124.8, 123.5, 123.4, 121.9, 121.8, 117.6, 117.4, 117.1, 116.9; FTIR (KBr pellet): ν 2022, 1906 cm^{-1} (metal carbonyl CO stretching). UV-vis ($CHCl_3$): λ_{max} (ε) = 508 nm (9000 $dm^3\ mol^{-1}cm^{-1}$). MS (FAB-MS): *m/z*: 675 $[M]^+$, 640 $[M\text{-}Cl]^+$. Anal. Calc. for $C_{27}H_{14}N_2ClF_2O_3Re$: C, 48.11; H, 2.09; N, 4.16. Found: C, 47.83; H, 1.96; N, 4.23 %.

Chlorotricarbonyl bis((4-trifluoromethyl)phenylimino)acenaphthene rhenium(I) ***4e***: (92 %). ^1H NMR (400 MHz, $CDCl_3$): δ 8.14 (d, J = 8.3 Hz, 2H), 7.93 (d, J = 8.5 Hz, 4H), 7.87 (d, J = 8.4 Hz, 2H), 7.57 (t, J = 7.8 Hz, 2H), 7.50 (d, J = 7.3 Hz, 2H), 6.99 (d, J = 7.3 Hz, 2H). ^{13}C NMR (125 MHz, DMSO-d_6): δ 196.8, 185.9, 173.6, 151.3, 144.9, 132.3, 131.1, 129.0, 128.4, 125.2, 124.8, 122.8, 121.8, 121.3, 112.7. FTIR (KBr pellet): ν = 2028, 1930, 1897 cm^{-1} (metal carbonyl CO stretching). UV-vis ($CHCl_3$): λ_{max} (ε) = 517 nm (4100 $dm^3\ mol^{-1}cm^{-1}$). MS (FAB-MS): *m/z*: 774 $[M]^+$, 739 $[M\text{-}Cl]^+$. Anal. Calc. for $C_{29}H_{14}N_2ClF_6O_3Re$: C, 45.00; H, 1.82; N, 3.62. Found: C, 44.73; H, 1.77; N, 3.27 %.

4.4. Measurements

^1H and ^{13}C NMR spectra (^1H NMR 298 K, ^{13}C NMR 298 K) were collected on a Bruker AM-500 (500-MHz), a Bruker AV-400 (400-MHz) or a Bruker DPX-300 (300-MHz) multinuclear Fourier transform nuclear magnetic resonance (NMR) spectrometers. Chemical shifts (δ) are reported in ppm relative to tetramethylsilane (TMS) as the internal standard and coupling constants (J) in Hz. Multiplicities are reported as singlet (s), doublet (d), triplet (t), quartet (q), and multiplet (m). Fourier transform infrared (FTIR) spectra were recorded as KBr pellet on a Bio-Rad FTS-7

FTIR spectrometer (4000 - 400 cm^{-1}) and are reported in cm^{-1}. UV-visible absorption spectra were recorded on a Hewlett-Packard 8452A diode array UV-visible spectrophotometer or a Varian Cary 50 UV-visible spectrophotometer. Positive ion FAB mass spectra were recorded on a Finnigan MAT95 mass spectrometer. Thermal analyses were performed on Perkin Elmer TGA7 thermal analyzers. The thermogravimetric analysis (TGA) was performed under a nitrogen atmosphere with the heating rate of 15 $^{\circ}C$ min^{-1}. Cyclic voltammetry (CV) was performed on a Princeton Applied Research 270 potentiostat. A conventional three-electrode system was adopted, which consisted of a glassy carbon working electrode and two platinum electrodes as the counter and reference electrodes. The salt bridges of reference electrode and counter electrode compartments were separated from the working electrode compartment by a vycor glass. Cyclic voltammograms were recorded at a scan rate of 100 mV/s. HPLC grade acetonitrile was used as the solvent and tetrabutylammonium tetrafluoroborate (0.1 M) was used as the supporting electrolyte. Ferrocene was added as the internal standard. For the DFT calculations, Gaussian98 program was used. The density functional theory calculations for the ground state of the complexes were performed by using B3LYP method with a LanL2DZ basis set.

4.5 Carrier Mobility Measurements

The thin film for charge carrier mobility measurement was fabricated by evaporating the material on an ITO coated glass substrate under vacuum. Typical thickness of the thin film was approximately 500 nm. A layer of 100 nm metal electrode was coated on the organic film surface by thermal evaporation. Charge carrier mobility was determined by the time-of-flight experiment.[31] A Laser Science VSL-337 nitrogen laser was used to generate a pulsed laser source (wavelength =337 nm, pulse energy

=120 μJ, and pulse width full width at half-maximum (fwhm) =3 ns). The transient photocurrent profiles was recorded with an oscilloscope (Tektronix TDS 3052B).

4.6 Photovoltaic Device Characterizations

The ITO coated glass substrates with sheet resistance of 15 Ω/square (Tinwell Technology Ltd.) were cleaned prior to use. The substrates were rinsed with toluene, ethanol, and acetone in sequence. It was then cleaned in an ultrasonic bath for 8 minutes in a 3 % Decon 90 glass-detergent solution, 8 minutes in ultrapure water (18.2 MΩ), 5 minutes in ethanol, and 5 minutes in acetone in sequence. The substrates were rinsed thoroughly with ultrapure water after each cleaning step. All the solvents used for cleaning were analytical grade. The substrates were dried under a nitrogen atmosphere. Before the ITO substrates were loaded into an evaporator, it was treated with UV ozone for 15 minutes. The multilayer photovoltaic devices were fabricated by evaporating different organic materials on the ITO coated glass substrates inside a vacuum chamber (10^{-6} mbar). Before evaporation, the rhenium complexes were purified by sublimation. The complex:C_{60} mixed layer was prepared by evaporating different materials from independent sources, which were monitored by individual sensor (Sigma SQC-222 CoDeposition Controller). A layer of aluminium electrode (active area = 3.1 mm^2) was deposited on the top of multilayer films by thermal evaporation.

The current-voltage characteristics of photovoltaic devices were recorded on a Keithley 2400 source meter. An Oriel 6255 Xenon lamp (150 W) equipped with an AM 1.5 filter that simulated solar radiation was used as the light source. The irradiation light intensity was measured by a Molectron Power Max 500D laser power meter and the film thickness was measured with a Vecco Dektak-3ST surface

profilometer. For the measurement of IPCE, a different wavelength of light was selected with a Thermo Oriel Corner Stone monochromator. The photocurrent generated was measured with a Keithley 2400 source meter. The light intensity was measured with a Newport 1830-C optical power meter equipped with an 818-UV detector probe.

Acknowledgements

The work reported in this paper has been substantially supported by the Research Grants Council of The Hong Kong Special Administrative Region, China (Project Numbers HKU7008/07P, HKU2/05C). Financial supports from the Strategic Research Theme, University Development Fund For Clean Energy Research (administrated by The University of Hong Kong) are also acknowledged.

References

[1] B. C. Thompson, J. M. J. Frechet, Angew. Chem. Intl. Ed. 47 (2008) 58.

[2] S. Günes, H. Neugebauer, N. S. Sariciftci, Chem. Rev. 107 (2007) 1324.

[3] M. Gratzel, J. Photochem. Photobio. C Photochem. Rev. 4 (2003) 145.

[4] M. Gratzel, MRS Bull. 30 (2005) 23.

[5] Y. Saito, T. Azechi, T. Kitamura, Y. Hasegawa, Y. Wada, S. Yanagida, Coord. Chem. Rev. 248 (2004) 1469.

[6] A. S. Polo, K. Itokazu, N. Y. M. Iha, Coord. Chem. Rev. 248 (2004) 1343.

[7] W. Y. Wong, X. Z. Wang, Z. He, A. B. Djurisic, C. T. Yip, K. Y. Cheung, H. Wang, C. S. K. Mak, W. K. Chan, Nature Mater. 6 (2007) 521.

[8] W. Y. Wong, X. Z. Wang, Z. He, K. K. Chan, A. B. Djurisic, K. Y. Cheung, C. T. Yip, A. M. C. Ng, Y. Y. Xi, C. S. K. Mak, W. K. Chan, J. Am. Chem. Soc. 129 (2007) 14372.

[9] C. W. Tse, K. Y. K. Man, K. W. Cheng, C. S. K. Mak, W. K. Chan, C. T. Yip, Z. T. Liu, A. B. Djurisic, Chem. Eur. J. 13 (2007) 328.

[10] K. W. Cheng, C. S. K. Mak, W. K. Chan, A. M. C. Ng, A. B. Djurisic, J. Polym. Sci. Part A: Polym. Chem. 46 (2008) 1305.

[11] W. Y. Wong, Macromol. Chem. Phys. 209 (2008) 14.

[12] P. K. Ng, X. Gong, S. H. Chan, L. S. M. Lam, W. K. Chan, Chem. Eur. J. 7 (2001) 4358.

[13] K. Y. K. Man, C. W. Tse, K. W. Cheng, A. B. Djurisic, W. K. Chan, J. Inorg. Organomet. Polym. Mater. 17 (2007) 223.

[14] N. A. Anderson, T. Lian, Coord. Chem. Rev. 248 (2004) 1231.

[15] H. L. Wong, L. S. M. Lam, K. W. Cheng, K. Y. K. Man, W. K. Chan, C. Y. Kwong, A. B. Djurisic, Appl. Phys. Lett. 84 (2004) 2557.

[16] H. L. Wong, C. S. K. Mak, W. K. Chan, A. B. Djurisic, Appl. Phys. Lett. 90 (2007) 081107.

[17] G. Knor, M. Leirer, T. E. Keyes, J. G. Vos, A. Vogler, Eur. J. Inorg. Chem. (2000) 749.

[18] R. V. Asselt, C. J. Elsevier, W. J. J. Smeets, A. L. Spek, R. Benedix, Recl. Trav. Chim. Pays-Bas 113 (1994) 88.

[19] J.-W. Kang, D.-S. Lee, H.-D. Park, Y.-S. Park, J. W. Kim, W.-I. Jeong, K.-M. Yoo, K. Go, S.-H. Kimb, J.-J. Kim, J. Mater. Chem. 17 (2007) 3714.

[20] V. M. Miskowski, V. H. Houlding, C. M. Che, Y. Wang, Inorg. Chem. 32 (1993) 2518.

[21] X. Gong, P. K. Ng, W. K. Chan, Adv. Mater. 10 (1998) 1337.

[22] W. K. Chan, X. Gong, W. Y. Ng, Appl. Phys. Lett. 71 (1997) 2919.

[23] T. Stubinger, W. Brutting, J. Appl. Phys. 90 (2001) 3632.

[24] W. Riess, H. Riel, T. Beierlein, W. Brutting, P. Muller, P. F. Seidler, IBM J. Res. Dev. 45 (2001) 77.

[25] Y. Shirota, Y. Kuwabara, H. Inada, T. Wakimoto, H. Nakada, Y. Yonemoto, S. Kawami, K. Imai, Appl. Phys. Lett. 65 (1994) 807.

[26] S. Uchida, J. G. Xue, B. P. Rand, S. R. Forrest, Appl. Phys. Lett. 84 (2004) 4218.

[27] P. Sullivan, S. Heutz, S. M. Schultes, T. S. Jones, Appl. Phys. Lett. 84 (2004) 1210.

[28] J. Drechsel, B. Mannig, F. Kozlowski, M. Pfeiffer, K. Leo, H. Hoppe, Appl. Phys. Lett. 86 (2005.

[29] T. Mori, K. Kato, J. Photopolym. Sci. Tec. 20 (2007) 61.

[30] M. Gasperini, F. Ragaini, S. Cenini, Organometallics 21 (2002) 2950.

[31] J. C. Scott, L. T. Pautmeier, L. B. Schein, Phys. Rev. B 46 (1992) 8603.

Table 1. Properties of complexes **4a-e**.

Complex	R	T_d (°C)	CH_3CN	$CHCl_3$	THF	Toluene	Thin Film	HOMO	LUMO
4a	OCH_3	336	464	493	493	514	475	-5.84	-3.73
4b	CH_3	345	474	499	502	517	500	-5.83	-3.75
4c	H	333	477	503	505	521	503	-5.83	-3.77
4d	F	346	480	508	508	523	508	-5.85	-3.81
4e	CF_3	253	482	517	513	549	516	-5.89	-3.92

Table 2. Hole and electron carrier mobilities of different complexes measured under an applied electric field strength of 300 kV/cm.

Complex	Hole carrier mobility μ_h (10^{-4} $cm^2V^{-1}s^{-1}$)	Electron carrier mobility μ_e (10^{-4} $cm^2V^{-1}s^{-1}$)
4a	2.9	3.4
4b	4.2	3.6
4c	19	17
4d	3.5	3.9
4e	2.5	4.8

Table 3. Performance of heterojunction devices ITO/HTM(10 nm)/**4c**/C_{60}(10 nm)/Al(60 nm) with different hole transport material (HTM) and active layer thickness.

Complex thickness (nm)	HTM	J_{sc}(mAcm^{-2})	V_{oc} (V)	FF	η_p (%)
15	CuPc	0.69	0.44	0.32	0.10
25	CuPc	0.59	0.48	0.39	0.11
35	CuPc	0.59	0.44	0.29	0.07
40	CuPc	0.15	0.42	0.16	0.01
50	CuPc	0.17	0.45	0.28	0.02
25	TPD	0.14	0.44	0.36	0.02
25	NPB	0.11	0.60	0.33	0.02

Table 4. Effect of complex **4c**:C_{60} ratio and active layer thickness to the performance of the devices ITO/CuPc/**4c**:C_{60}/C_{60}/Al.

Entry	**4c**:C_{60} ratio	thickness of (**4c**:C_{60}) layer	J_{sc}(mAcm^{-2})	V_{oc} (V)	FF	η_p (%)
1	1:9	25	4.13	0.37	0.49	0.74
2	1:9	50	2.67	0.37	0.40	0.40
3	1:9	75	1.48	0.30	0.39	0.17
4	1:9	100	2.30	0.3	0.46	0.31
5	3:7	25	4.03	0.42	0.45	0.76
6	3:7	50	2.72	0.44	0.52	0.62
7	3:7	75	2.93	0.46	0.43	0.58
8	3:7	100	0.03	0.30	0.12	0.01
9	1:1	25	3.0	0.47	0.33	0.46
10	1:1	50	5.07	0.51	0.51	1.29
11	1:1	75	4.34	0.42	0.42	0.76
12	1:1	100	3.23	0.46	0.32	0.47
13	9:1	50	1.3	0.59	0.20	0.15

Table 5. Performance of photovoltaic cells with different rhenium complexes, hole transport material (HTM), and exciton blocking layer (EBL) ITO/HTM (10 nm)/Complex:C_{60} (1:1) (50 nm)/C_{60} (10 nm)/EBL (10 nm)/Al (60 nm).

Entry	Complex	HTM	EBL	J_{sc}(mAcm^{-2})	V_{oc} (V)	FF	η_p (%)
1	**4a**	CuPc	-	3.25	0.46	0.53	0.79
2	**4b**	CuPc	-	2.84	0.52	0.50	0.73
3	**4c**	CuPc	-	5.07	0.51	0.51	1.29
4	**4d**	CuPc	-	2.76	0.47	0.48	0.62
5	**4e**	CuPc	-	2.70	0.44	0.54	0.64
6	**4c**	ZnPc	-	2.41	0.48	0.51	0.59
7	**4c**	TPD	-	0.20	0.48	0.36	0.035
8	**4c**	NPB	-	0.38	0.72	0.29	0.08
9	**4c**	CBP	-	0.014	0.34	0.26	0.01
10	**4c**	CuPc	BCP	0.18	0.30	0.51	0.27
11	**4c**	CuPc	BCP/Ag*	0.21	0.40	0.54	0.45
12	**4c**	CuPc	BCP/Mg:Ag (6:1)*	2.59	0.44	0.46	0.53
13	**4c**	CuPc	PTCDI	0.038	0.66	0.18	0.004

* Aluminium electrode was not deposited in these devices.

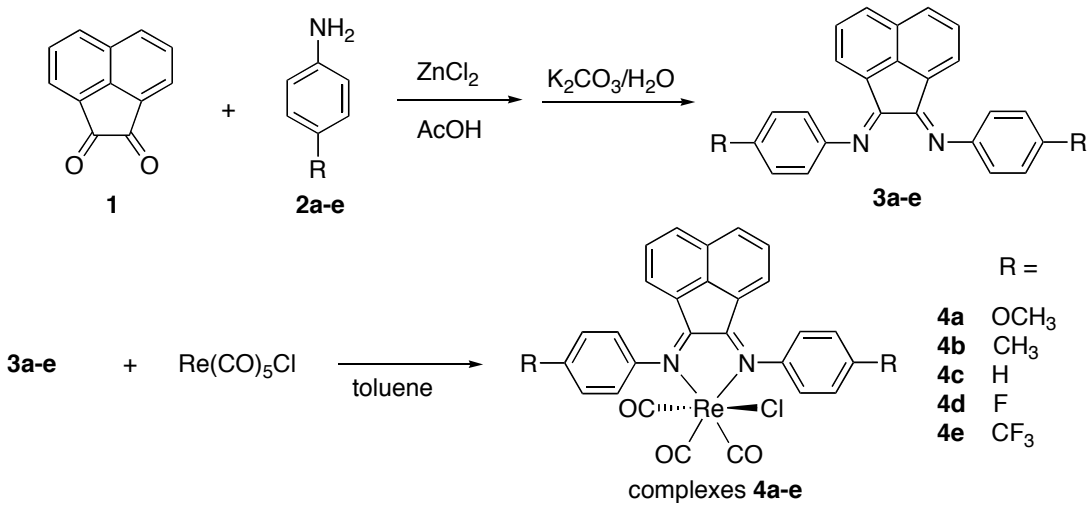
NH2
ZnCl2
AcOH
K2CO3/H2O
O
O
R
1
2a-e
3a-e
3a-e
Re(CO)5Cl
toluene
OC
Re
Cl
OC
CO
complexes 4a-e
R =
4a OCH3
4b CH3
4c H
4d F
4e CF3

Scheme 1.

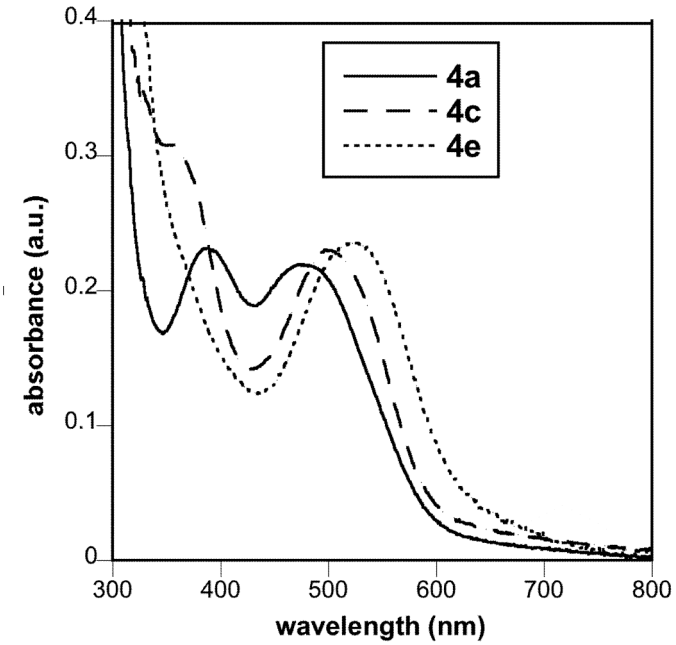

Figure 1. UV-vis absorption spectra of rhenium complexes in $CHCl_3$.

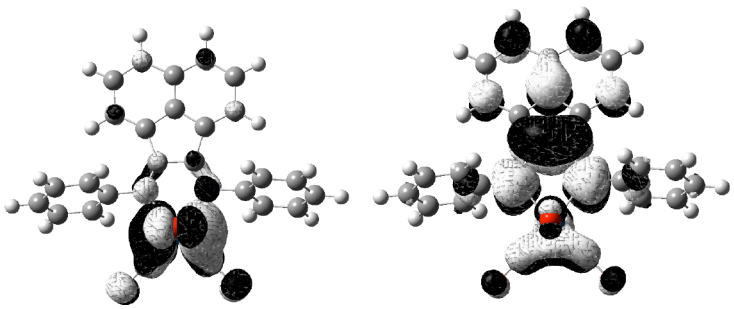

Figure 2. Calculated wave functions for the HOMO (left) and LUMO (right) of complex **4c**.

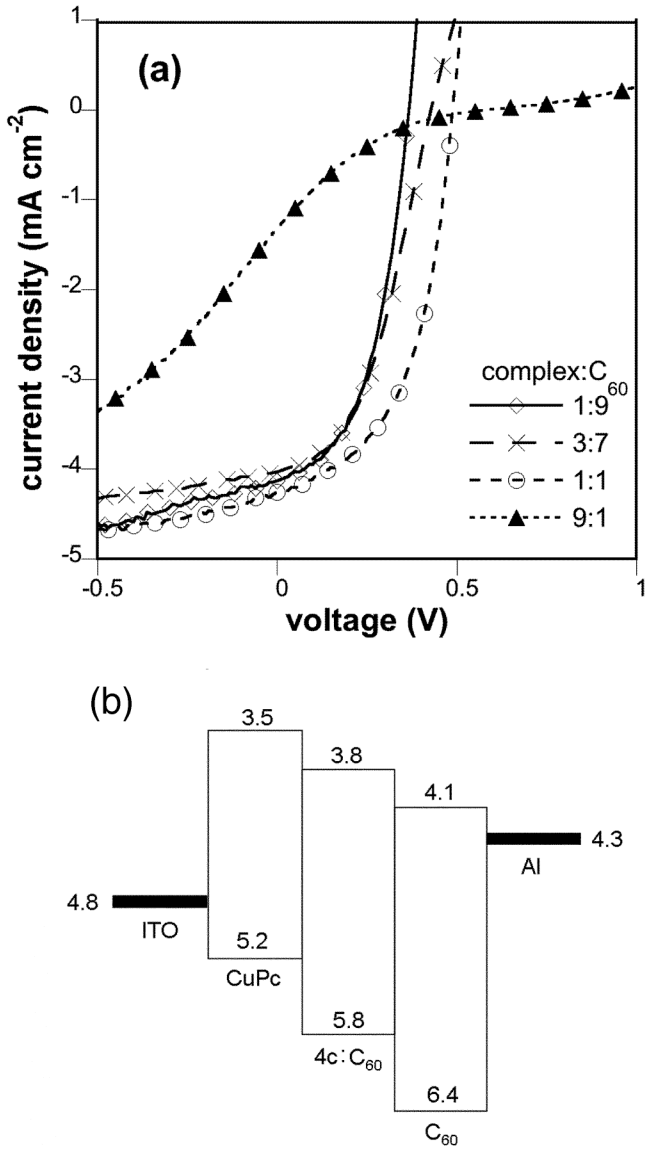

Figure 3. (a) Current-voltage characteristics of the device ITO/CuPc/**4c**:C_{60}/C_{60}/Al with different complex:fullerene ratios under illumination of simulated AM1.5 solar light. (b) Schematic diagram showing the energy levels (in eV) of different materials in the device.

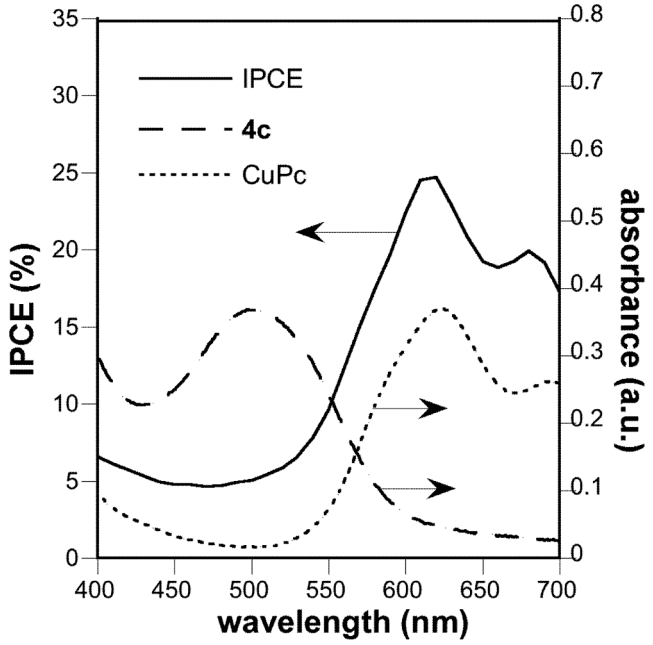

Figure 4. Plot of IPCE as the function of wavelength for the device ITO/CuPc/**4c**:C_{60} (1:1)/C_{60}/Al under illumination of simulated solar light. The absorption spectra of thin films of **4c** and CuPc are also shown.